Synthesis of Quadband mm-Wave Microstrip Antenna Using Genetic Algorithm for Wireless Application

Arebu Dejen [1,*] , Jeevani Jayasinghe [2], Murad Ridwan [1] and Jaume Anguera [3,4,*]

1   School of Electrical and Computer Engineering, AAit, Addis Ababa University, Addis Ababa 1000, Ethiopia
2   Department of Electronics, Wayamba University of Sri Lanka, Kuliyapitiya 60200, Sri Lanka
3   Telecommunication Engineering, Universitat Ramon LLull, 08022 Barcelona, Spain
4   Ignion, 08174 Barcelona, Spain
*   Correspondence: arbdjn@gmail.com (A.D.); jaume.anguera@salle.url.edu (J.A.)

Abstract: Antennas with multifunctional capabilities integrated into a single device that demonstrates a high performance are in demand, and microstrip antennas with quadband coverage are very useful for a wide range of mm-wave applications. Antennas and propagation at mm-wave frequencies, on the other hand, poses several challenges which can be overcome by applying performance enhancement techniques to meet design objectives. This article presents the use of a binary-coded genetic algorithm for developing an improved quadband mm-wave microstrip patch antenna. The patch shape was optimized by dividing a conducting surface into 6×6 tiny rectangular blocks. The algorithm generated the solution space by introducing conducting and nonconducting features for each radiating cell on the patch surface and then greedily searched for the best-fitted individual based on the cost function. With the combination of High-Frequency Structure Simulator (HFSS) and MATLAB, candidate antennas were iteratively modeled by applying the suggested algorithm. The optimized antenna resonated at four frequencies centered at 28.3 GHz, 38.1 GHz, 46.6 GHz, and 60.0 GHz. The antenna realized a peak broadside directivity of 7.8 dB, 8.8 dB, 7.3 dB, and 7.1 dB, respectively, with a total operating bandwidth of 11.5 GHz. The research findings were compared with related works presented in the literature and found that the optimized antenna outperformed them in terms of bandwidth, directivity, and efficiency.

Keywords: genetic algorithm; microstrip antenna; mm-wave antenna; quadband antenna

1. Introduction

There is no doubt that wireless communication is one of the fastest-growing and most dynamic areas in the telecommunications industry. In particular, mobile communication has evolved significantly before reaching the current generation. Despite the fact that high data rate demands in mobile broadband were met by the LTE released technology, the exponential growth of data rate requirements has been driven by the dynamically vast number of wireless devices. In these communication technologies, more and more bandwidth-intensive applications are emerging. Millions of wireless devices, including HD TVs, cameras, laptops, household appliances, smartphones, sensors, video surveillance systems, wearable devices, and robots, will be able to connect, with an exponential growth expected soon. Simultaneously, technologies related to smart grids, smart cities, virtual reality, the Internet of things (IoT), machine-to-machine communication, autonomous driving, and e-health are emerging [1]. These new and developing technologies need tremendous bandwidth to enable the simultaneous movement of massive volumes of data. Because of bandwidth constraints, the existing microwave spectrum does not include all of these elements, but millimeter wave (mm-wave) frequencies offer ample capacity and are projected to meet such high-end needs.

The mm-wave frequency band offers the required bandwidth for these applications. However, this band has a myriad of difficulty, including significant propagation losses,

blockages, and atmospheric losses [2]. Since an antenna is essential for any wireless link and its operational effectiveness is greatly dependent on the design, the antenna design community has made significant advances in technology to fulfill the ongoing demand of consumers by addressing associated issues and concerns. Aside from these concerns, while considering mobile and sensor network devices in mm-wave communication, the proposed antenna must be energy efficient and function with minimal energy [3]. Antennas for mm-wave signal propagation should be high-gain and directional from both user equipment and base station terminal to avoid shadowing losses, path losses, and multipath fading for successful mm-wave communication [4]. Furthermore, wide-bandwidth antennas are also necessary for the optimum usage of the available spectrum in the mm-wave band, which will provide a high data rate [5]. Thus, it is vital to work on the optimization of antenna technology in order to overcome the propagation challenges and maximize the multifunctionality, bandwidth, gain, and directivity of mm-wave antennas [6].

In recent years, several research articles have reported on mm-wave antenna design for the fifth-generation network devices. These antenna devices must have a low profile, planar construction, and multiband capabilities. Microstrip patch antenna technology has become an appealing alternative, because of its low profile, cheap cost, simple configuration, and ease of fabrication [7]. Traditional microstrip patch antennas, on the other hand, have a limited bandwidth, low gain, and poor directivity [8,9]. Extensive research has been done to enhance the performance of microstrip antennas in terms of bandwidth, gain, and directivity by various mechanisms. Stacked-based wideband microstrip antennas for 5G and 6G applications using particle swarm optimization were presented [10]. In reference [11], a circularly polarized omnidirectional patch antenna was proposed for 5G machine-to-machine communication. For patch antenna performance enhancement, a square-shaped metasurface was mounted above the radiating patch [12]. To boost spectral efficiency, a switchable beam for mm-wave communication was proposed by integrating PIN diodes at the ground [13]. By using cooperative feeding, a linear array was also proposed to attain a high gain for the mm-wave patch antenna [14]. In addition, other mechanisms have been used in the literature to improve the radiation characteristics of microstrip antennas for mm-wave devices, such as electromagnetic band gap structures (EBG) [15], defected ground surface (DGS) structures [16], frequency-selective surfaces (FSS) [17], and near-zero-index metamaterial structures [18].

Good multiband antenna performance is necessary to accommodate many wireless services spread across a wide frequency range [19,20]. The inclusion of many communication protocols in a single compact system has piqued the interest of many researchers [21]. However, as an antenna is a hardware device that operates on a fixed resonance frequency, there are a few critical limitations in exploring other working bands. Even though the multiband functioning of an antenna is accomplished via the use of various techniques, it is difficult to achieve a high performance while clearing bandwidth constraints and meeting possible gain in all coverage bands with a compact antenna size in classical antenna design technologies and conventional antennas. Numerous mechanisms employed in advancing a patch antenna for quadband operation have been published in the literature. A quadband antenna for mobile communication was designed by a combination of three quarter-wavelength monopole antennas resonating at 0.4 GHz, 0.9 GHz, 1.6 GHz, and 2.75 GHz [22]. A compact microstrip antenna with three L stubs and a combination of inverted L and T stub shapes resonating at 2.54/3.5/4.38/5.3 GHz quadband frequencies was reported in [23]. Circularly polarized quadband antenna was proposed by integrating a ring, stubs, and an open-ended C-shaped slot in the ground surface was presented [24]. A quadband antenna which resonated at 1.78 GHz, 3.28 GHz, 4 GHz and 4.3 GHz was configured by using a metamaterial-inspired defected ground structure in [25]. A quadband mm-wave dielectric resonator antenna propagating at 28 GHz, 34 GHz, 38 GHz, and 42 GHz with enhanced gain was proposed in [26]. In [27], the authors introduced a four-port quadband mm-wave MIMO antenna that resonated at 28 GHz, 43 GHz, 52 GHz, and 57 GHz. A multiband circularly polarized planar antenna operating at 28 GHz, 38 GHz,

60 GHz, and 73 GHz for 5G and WiGig applications by applying a square-slot antenna fed by a proximity-coupled microstrip line and loaded by a grounded square loop and three tilted angle strips was reported in [28] and a similar design using a cross-slot on the patch for multiband operation was described in [29]. These methods were sophisticated, and the corresponding proposed antennas also had a complicated structure. Multiband antennas were modeled using a variety of optimization algorithms such as autocontext broad learning system [30], deep Gaussian process model [31], and genetic algorithms [32]. The author of [33] described a multiband antenna at mm-wave frequency that employed a binary-code genetic algorithm with a rectangular cell. Further improvement on the performance of mm-wave antennas by using autonomous optimization algorithms is essential and a challenging research field.

In contrast, this research presents a quadband patch antenna improvement for mm-wave frequencies with increased gain, impedance bandwidth, and directivity utilizing a binary-coded genetic algorithm. The algorithm was employed on the patch surface by manipulating the gridded rectangular cells to generate different shapes. High-Frequency Structure Simulator (HFSS) software in combination with MATLAB was used to examine and simulate the proposed antenna. MATLAB was employed to write and analyze the authors' defined binary-coded genetic algorithm. Since HFSS can read VBS code, the algorithm repeatedly delivered the information of the newly created individual antennas and saved them in the form of a Visual Basic Script (VBS) file. Then, HFSS invoked the created VBS file and converted the details of the antenna parameters into the antenna model and validated it. HFSS simulated and computed the modeled antenna performance for specific parameters. The resulting performance of each individual antenna was immediately exported to the main genetic algorithm function in MATLAB. At each computation, the antenna performance was sent to the genetic algorithm optimizer code, which was written in MATLAB. The algorithm began evaluating the fitness function, ranking the individuals based on the fitness value, and picking the parents for the next generation.

2. Antenna Modeling

Despite certain drawbacks, the microstrip patch antenna is likely the most successful and groundbreaking antenna technology since it offers various significant advantages over other types of antennas. The substrate, radiating patch, and ground plane are the three fundamental layers of a microstrip antenna. It can be built as a metallic patch on top of the dielectric substrate, with a ground plane beneath the dielectric layer. In the design of a microstrip antenna, the radiating patch can have a variety of geometries. However, rectangular and square patch antennas are the most frequent due to their simplicity of analysis and fabrication, as well as their appealing radiation properties. In this antenna modeling, a proposed microstrip patch antenna was designed on a 15 mm × 15 mm size RT/duriod-5880(tm) substrate. It is a dielectric substance designed for better electrical and mechanical stability in radiating patches. It can also assist in the generation of displacement current, which generates a magnetic field that changes over time. The substrate has a 2.2 dielectric constant, 0.0009 tangent loss, and 0.5 mm thickness. The initial dimensions of the reference model were calculated using the standard formula presented in [34]. However, the antenna with the estimated dimensions did not have sufficient antenna performance at the desired frequency bands. Therefore, a parametric study was used to fine-tune the dimensions of the radiating patch. Accordingly, the patch's length was varied in four stages from 7.6 to 8.2 mm, while its width was adjusted in 0.2 mm step sizes from 9.2 to 9.8 mm. When the antenna resonated and performed well around 38 GHz, the optimal patch length was 0.73 λ and the patch width was 0.9 λ. The microstrip line-feeding technique was used in this research because it is straightforward to analyze and easy to build utilizing photoetched technology on dielectric material to excite the radiating patch. A 50 Ω microstrip feed line with dimensions of 3.4 mm × 0.9 mm was connected to the patch. A designed feed line employed a two-stage transition for impedance matching. The reference antenna model and its optimal size are presented in Figure 1. It was used for the patch geometry

optimization with a binary-coded genetic algorithm.
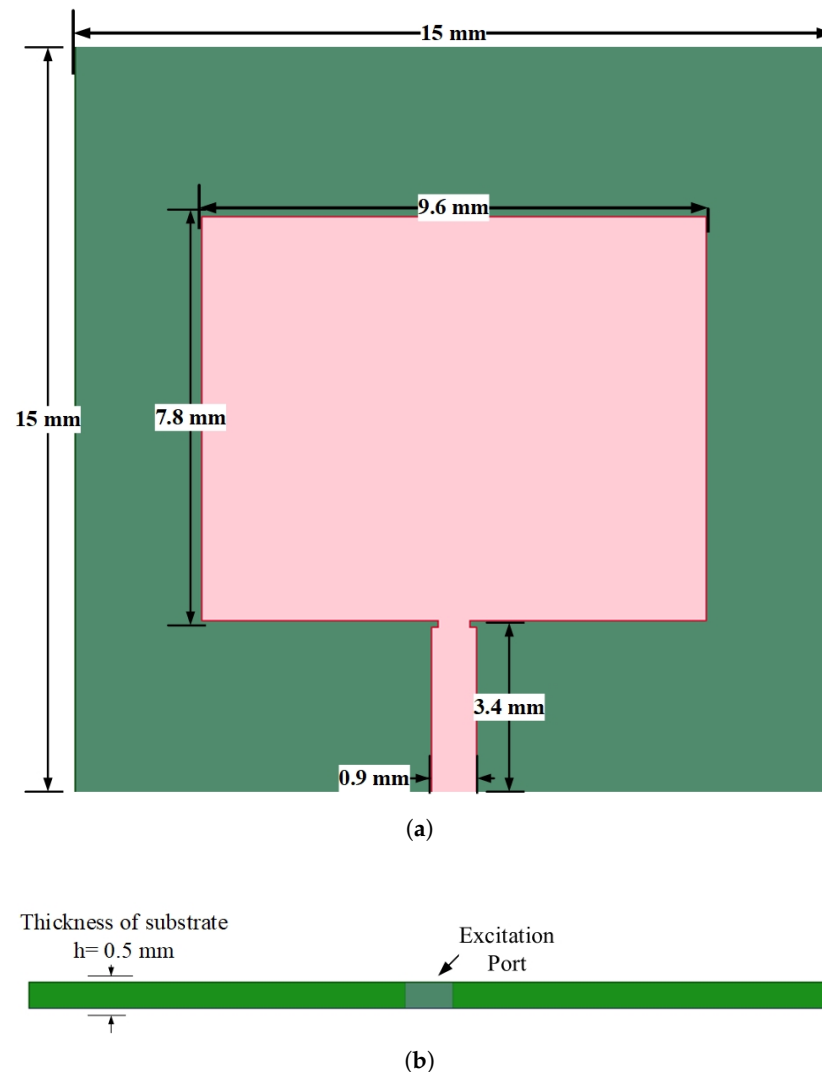
Figure 1. (**a**) Reference patch antenna model on a substrate (h = 0.5 mm, ϵ_r = 2.2, tanδ = 0.0009) (**a**) top view, (**b**) side view.

3. Optimization Procedure

Antenna optimization and design are influenced by several elements, including operating frequencies, size, radiation pattern, gain, directivity, and others. The employment of autonomous algorithms in antenna optimization has grown significantly to solve the intricate and continuously developing problem of antenna technologies. Optimization using genetic algorithm is based on natural selection whereas it selects the fittest individuals to create offspring for the next generation. It is a search technique that handles a large number of optimum and approximated solutions from the solution space. In a binary-coded genetic algorithm, a gene is a binary bit with a value of "1" or "0", the chromosome is a string of bits that represents an individual, and an individual is a single candidate solution drawn from the solution space [35]. In the search space, a population is a collection of individuals at any particular time. When the population size clustered as a single generation becomes large, the algorithm has more search space. However, it requires much more computational cost, memory, and time. The first generation is produced by a random process, while subsequent generations are produced by more fit and chosen individuals who have a higher likelihood of producing better offspring as reflected by the cost. Crossover and mutation operations are used to increase the population diversity [36].

The operator in charge of performing reproduction from two selected individuals is the crossover operator. In contrast, a mutation is used to increase the population diversity. This iterative technique produces successive generations until a stopping condition is met [37]. Figure 2 depicts a flowchart of the genetic algorithm implementation procedure applied in the antenna optimization.
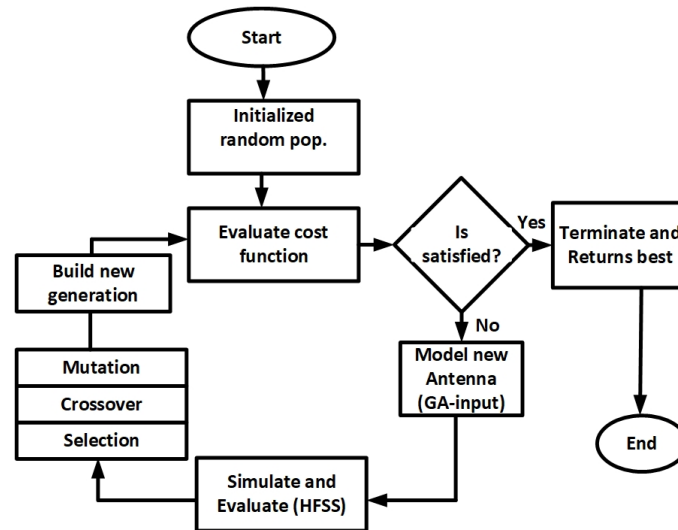
Figure 2. Flowchart of genetic algorithm implementation in antenna optimization.

The patch surface can be partitioned into several geometric forms, such as circular shapes, as seen in [19]. However, rectangular cells are ideal for addressing the entire patch surface with on and off characteristics. The number of genes on a chromosome has a significant impact on computing time, the number of potential candidate solutions in the search space, and the performance of best-fit individuals. For instance, the authors in [33] offered 8×8 gridded rectangular cells for a dual-band antenna optimization, while the authors in [38] also presented 10×10 cells for a triband antenna optimization. However, the main concern of this algorithm in our optimization was searching for the best-fitted individuals from the given solution space. As a consequence, the reference antenna's patch surface was divided into 6×6 small, random, and uniform rectangular cells to improve the patch shape, as shown in Figure 3.
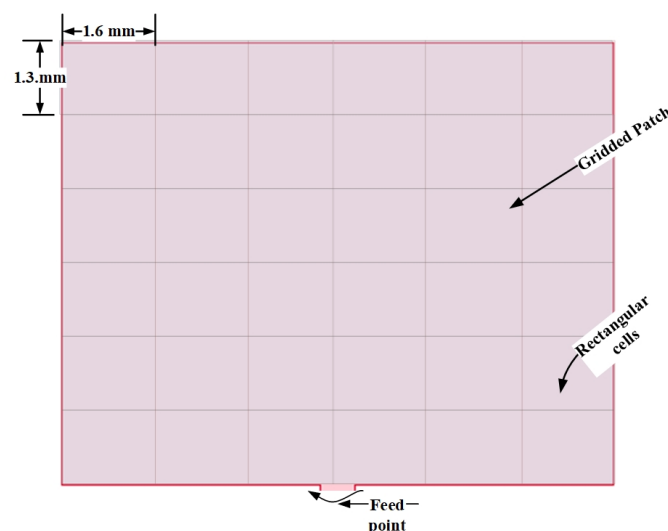
Figure 3. Placement of 36 rectangular cells on a rectangular patch surface.

A binary coding scheme defines each cell's conducting and nonconducting features. If the cell is conducting, a binary "1" is assigned to the associated gene, whereas a nonconducting gene is represented by a binary "0" [39]. The nonconducting surfaces were eliminated from the radiating patch sections, and the only geometry visible on the patch geometry was the combination of conducting cells. On each extensive iteration, the combination could generate a new structure of patch antenna. Following the establishment of these critical features of the genetic algorithm, the other critical component of the algorithm, the fitness function, should be specified. The fitness function may differ depending on the goals for which the antenna is optimized. The ultimate focus of this improvement is to create a single-element patch antenna that resonates at four unique mm-wave bands with an increased bandwidth at each band. When adopting $S_{11} \leq -10dB$ as the operational bandwidth, the cost function is intended to lower the reflection coefficient for each working band while increasing the operating bandwidth. As a result, the fitness function was developed as follows:

$$FitnessFunction = \frac{-1}{N} \sum_{i=1}^{N} S_{11}(f_i))$$ (1)

where $S_{11}(f_i)$ was designed as:

$$S_{11}(f_i) = \begin{cases} S_{11}(f_i) & if \quad S_{11}(f_i) \geq -10dB \\ -10dB & if \quad S_{11}(f_i) \leq -10dB \end{cases}$$ (2)

where N is the number of sample frequencies in each band, f_i is the sample frequency at each 100 MHz interval and $S_{11}(f_i)$ is the reflection coefficient of the antenna.

Table 1 organizes and summarizes the genetic algorithm optimization setup.

Table 1. Genetic algorithm optimization setup.

No.	Parameter	Values
1	Population size	30
2	Genes in a chromosomes	36
3	Maximum number of generations	100
4	Type of Crossover	Single-point
5	Crossover Probability	0.8
6	Mutation	Single-bit
7	Rate of Mutation	0.01
8	Selection method	Tournament

4. Results and Discussion

The simulation converged after 40 iterations, as shown in Figure 4a, and the iteration continued for the next 60 generations to demonstrate the consistency of the convergence. Finally, Figure 4b depicts the best-fitted individual antenna based on the algorithm. The solution space had a capacity of $2^{36} = 6.8 \times 10^{10}$ individuals in it. If the computing time of each individual design was 1 s, the overall computation time to find the best-fitting individual would be 2.1×10^3 years. However, owing to the application of the genetic algorithm, the best-fitted individuals were picked in only 40.3 h while utilizing a computer with a core I7, 8 GB RAM, and 2.7 GHz of processing speed.

(**a**)　　　　　　　　　　　　　　　　　　　　　　　　(**b**)
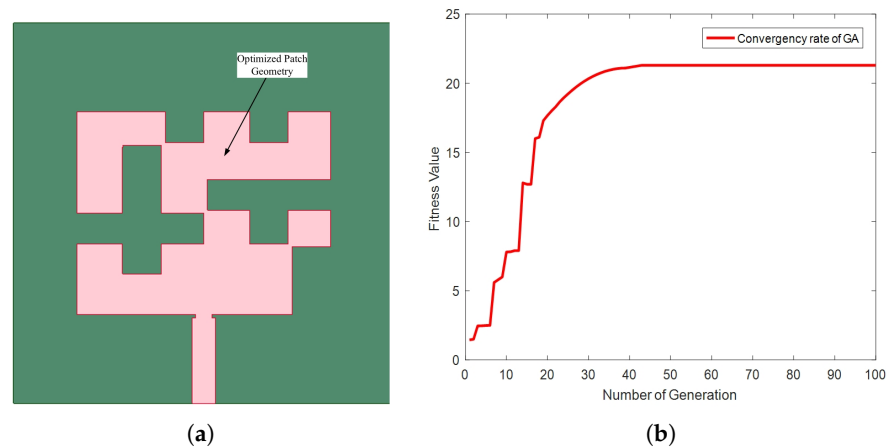
Figure 4. (**a**) Genetically optimized patch geometry, (**b**) average fitness value vs. number of generation.

Both the reference model and the genetically engineered antenna were simulated using ANSYS HFSS. The reference antenna resonated at a single frequency of 38 GHz and had a covered impedance bandwidth of 1.2 GHz. The peak S_{11} value of the reference model at 38 GHz was −38.4 dB, whereas the antenna's maximum directivity was 6.1 dB. Since the reference model was created using the idea of a traditional microstrip antenna model, the results were anticipated. On the other hand, the proposed genetically optimized antenna worked at four distinct frequencies: 28.3 GHz, 38.1 GHz, 46.6 GHz, and 60.0 GHz. The outcomes demonstrated that the antenna's bandwidth was also improved.

As shown in Figure 5, the antenna operated in a quadband, with a peak value of return loss S_{11} = −21.4 dB at 28.3 GHz, S_{11} = −18.1 dB at 38.1 GHz, S_{11} = −13.8 dB at 46.6 GHz, and S_{11} = −22.1 dB at 60.0 GHz. The lower the reflection coefficient value, the better the antenna's performance, which implied it reduced the reflected power to the source while increasing the radiated power from the surface. When S11 < −10 dB was taken into account, the bandwidth improvement of the antenna in the operating bands was visible. At a 28.3 GHz center frequency, the antenna had a fractional bandwidth of 3.2% or 0.9 GHz, 6.0% or 2.3 GHz, 3.4% or 1.6 GHz, and 11.1% or 6.7 GHz at 28.3, 38.1, 46.6, and 60.0 GHz, respectively. A total of 11.5 GHz of bandwidth was attained by the proposed antenna, and the bulk of the operating bands were situated close to the central frequency of 60 GHz. It is highly important for a number of bandwidth-hungry systems, such as wireless sensor networks and other short-range broadband applications that operate in that band.
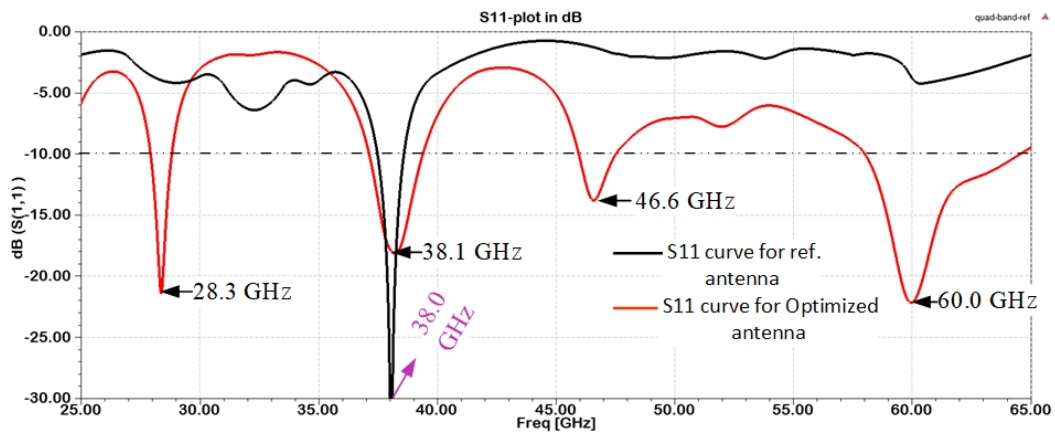
Figure 5. Simulated results of S_{11} for genetically optimized antenna and reference model.

All operational bands (27.9 GHz–28.8 GHz, 37.1 GHz–39.4 GHz, 45.9 GHz–47.5 GHz, and 57.8 GHz–64.5 GHz) had a voltage standing wave ratio (VSWR) of less than two. VSWR values at 28.3 GHz, 38.1 GHz, 46.6 GHz, and 60 GHz were, respectively, 1.18, 1.28, 1.51, and 1.45. As a result, it could be shown that there was a good chance of matching or just a slight mismatch loss at the antenna's feed in four resonant bands.

To have the maximum radiated power at the patch, the conjugate of the antenna input impedance and the transmission line characteristics impedance should be matched. Figure 6 displays the real and imaginary input impedance plot of the optimized antenna. By adjusting the transnational arm's length in the microstrip feed line and optimizing the patch design during each iteration, a maximum power transmission was attained in this paper. It demonstrated that there were only minor differences between the antenna's input impedance and the characteristic impedance of the transmission line. The input impedance of the engineered antenna was $44.31 + j5.64$ at 28.3 GHz, $44.10 − j10.28$ at 38.1 GHz, $65.65 − j18.39$ at 46.6 GHz, and $51.92 + j7.95$ at 60.0 GHz, as shown in Figure 6. Despite having a low reactance value, their real impedance value was close to the characteristic impedance. The findings indicated that the antenna and transmission line were nearly matched.
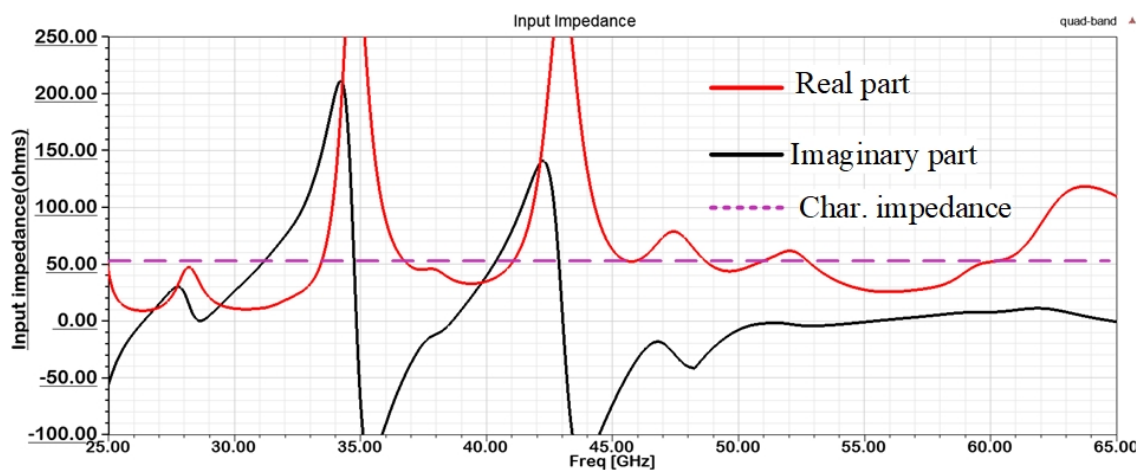
Figure 6. Real and imaginary input impedance plot versus frequency

The directivity and gain were better than those of the reference model and sufficient for mm-wave wireless applications. The antenna's 3D gain plot at four operational frequencies is shown in Figure 7. The antenna's maximum gain was 8.6 dB at 38.1 GHz. At 60.0 GHz, the optimized antenna minimum gain was observed as 6.9 dB, which was better than that of the conventional (reference) microstrip antenna model. The 3D gain pattern illustrated that its radiation pattern was almost broadside with slight distortions at a certain angle in higher-frequency bands (60.0 GHz). The optimized antenna also attained a 7.7 dB gain at 28.3 GHz and 7.2 dB at 46.6 GHz.

Figure 8 depicts the antenna's directivity pattern in the planes of $\theta = 0^0$ and $\phi = 90^0$, which was almost projected in a broadside orientation. Furthermore, a directivity enhancement in all working bands was observed. At 38.1 GHz, the maximum peak directivity of the optimized antenna was 8.8 dB at $\theta = 0^0$, while at 28.3 GHz, 46.6 GHz, and 60.0 GHz, peak broadside directivity values of 7.8 dB, 7.3 dB, and 7.1 dB were observed, respectively.
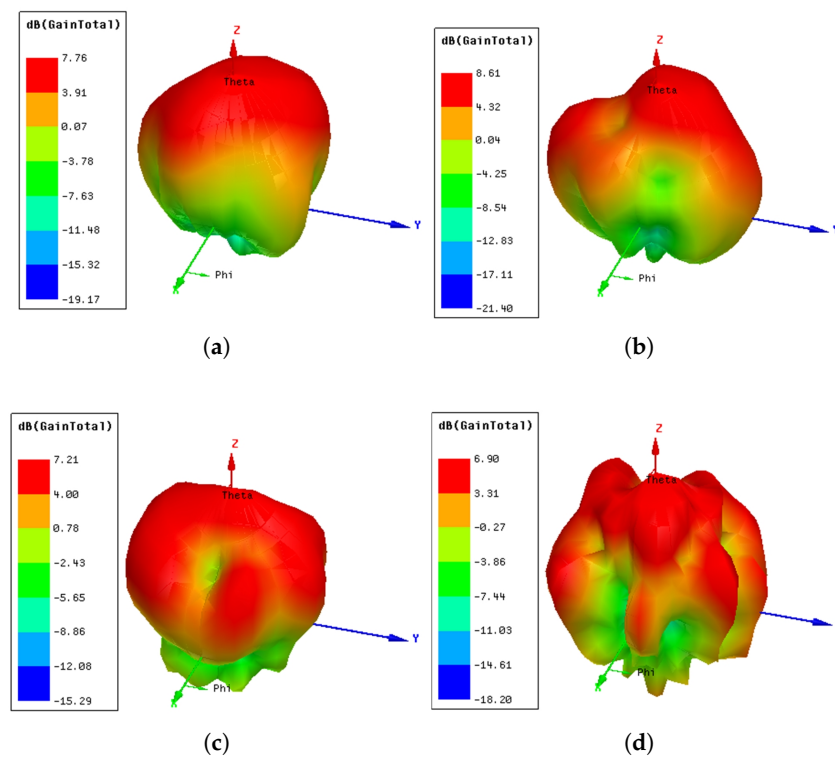
Figure 7. The 3D gain plot of the proposed antenna in dB (**a**) at 28.3 GHz, (**b**) at 38.1 GHz, (**c**) at 46.6 GHz, and (**d**) at 60.0 GHz.
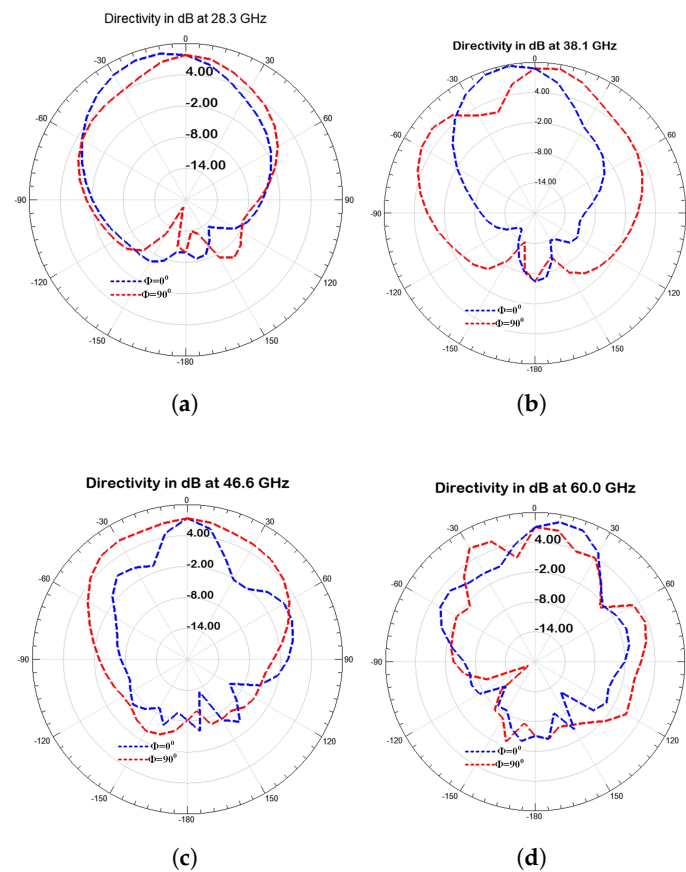
Figure 8. The 2D radiation pattern plot of the proposed antenna in dB (**a**) at 28.3 GHz, (**b**) at 38.1 GHz, (**c**) at 46.6 GHz, and (**d**) at 60.0 GHz.

The antenna's total efficiency and radiation efficiency are additional crucial metrics to describe an antenna's performance. The mismatch loss is not taken into consideration by the radiation efficiency; however, it is by the total efficiency, which is the product of the radiation efficiency and the mismatch loss. The radiation efficiency of the improved antenna was 96.3%, 95.4%, 97.7%, and 94.8%, respectively, at 28.3 GHz, 38.1 GHz, 46.6 GHz, and 60.0 GHz, as depicted in Figure 9. However, the mismatch loss at resonant frequencies had little impact on the overall efficiency. In light of this, the improved antenna had a total efficiency of 95.8 % at 28.3 GHz, 93.8% at 38.1 GHz, 93.4% at 46.6 GHz, and 94.2% at 60.0 GHz, respectively. The efficiency of an antenna determines how much energy is radiated or lost in terms of heat or in other ways. The optimized antenna received the maximum power from the sources available in accordance with the input impedance matching description, and the efficiency parameter also revealed that the received power immediately converted to radiation energy with minimal dissipation. This increased the antenna's energy efficiency and made the proposed antenna appropriate for mobile and sensor network in mm-wave wireless communication systems' quadband applications.
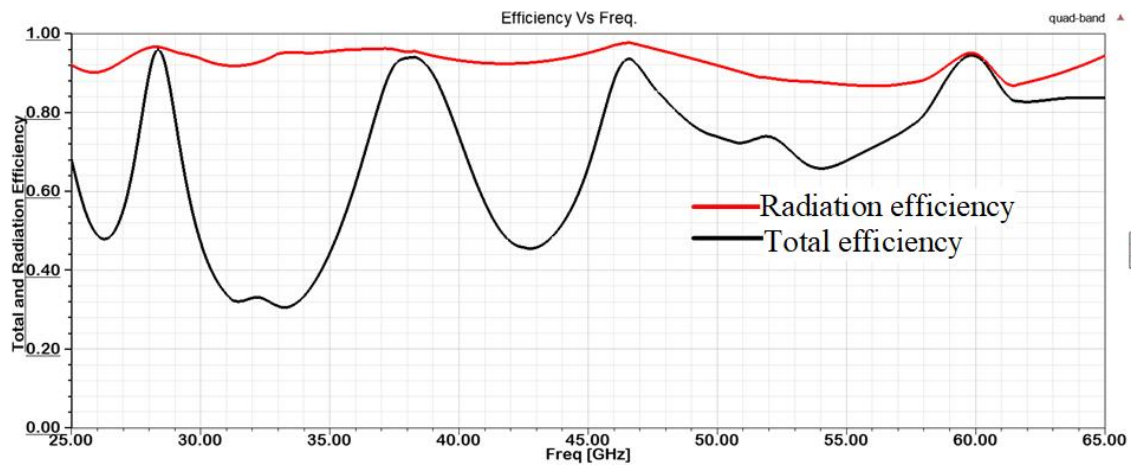
Figure 9. Total efficiency and radiation efficiency of the optimized antenna.

Figure 10 depicts the surface current distributions of the entire patch antenna to further clarify the quadband operation properties of the optimized antenna at 28.3, 38.1, 46.6, and 60.0 GHz. The graphic clearly shows that the current distributions differed across the four bands. The patch's surface's current distribution path enabled the antenna to resonate at various frequency bands. The majority of the current distributions were located near the feed point and the cell's edges on the optimized patch surface.

(**a**)   (**b**)
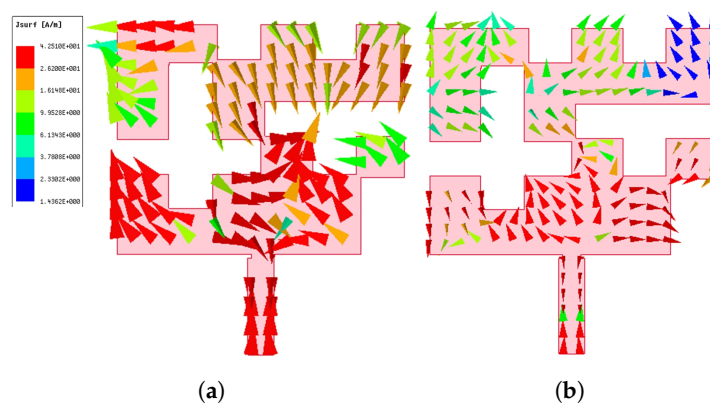
Figure 10. *Cont.*
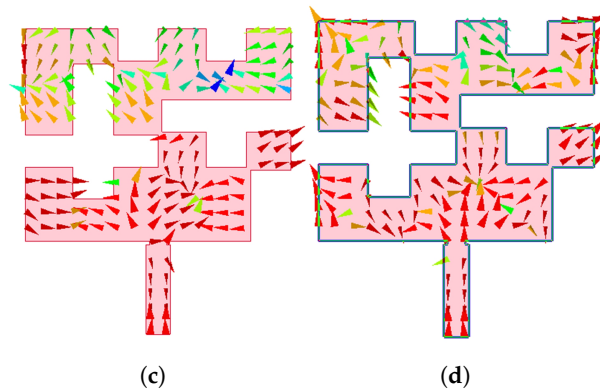
Figure 10. Surface current distribution of genetically optimized antenna (**a**) at 28.3 GHz, (**b**) at 38.1 GHz, (**c**) at 46.6 GHz, and (**d**) at 60.0 GHz.

5. Comparison with Related Works

Almost all of the related works mentioned in the literature employ a complex antenna structure to generate a quadband. For instance, [20,27] employed sophisticated superstrate and slots structures for quadband creation. In contrast, this work employed a very simple antenna structure that was simple to model and manufacture. The optimized antenna performance were compared with several relevant works in the literature, as shown in Table 2. Accordingly, a 4×4 hexagonal patch MIMO antenna operating in a quadband achieved a peak gain of 8.0 dB [27]. The bandwidth of the antenna, on the other hand, received less attention. At the same time, that antenna had a low directivity in comparison to that of this study. Furthermore, using a single optimized antenna, this study achieved a gain slightly higher than their maximum gain. A work presented in [23] achieved a peak gain of 1.98 dB in microwave frequencies, but the gain was significantly lower than that of our optimized antenna. To achieve quadband operation, the authors of [26] employed a dielectric resonator antenna (DRA) with a slotted ground plane and superstrate. The DRA achieved an overall antenna bandwidth of about 10 GHz. However, our proposed antenna outperformed the DRA by achieving a bandwidth broader than 11 GHz. When compared to previous relevant studies, the uniqueness of this work can be seen in the improvement of bandwidth, gain, and directivity of a single antenna with quadband frequency operation using a binary-coded genetic algorithm optimization. Moreover, the antenna performance is sufficient for mm-wave wireless communication.

Table 2. Performance comparison of the proposed antenna with other mm-wave antennas.

No.	Paper	Patch Size in λ^2	Resonant freq. (GHz)	BW in GHz ($S_{11} \leq -10$ dB)	Directivity (dB)	Gain (dB)	Techniques
1	[6]	0.74×0.79	28	0.3	6.7	-	U-shaped
			38	0.5	7.9	-	slot
2	[20]	0.47×0.46	28	0.84	7.3	6.8	Slotted
			38	0.37	7.5	7.2	patch
			61	0.9	6.9	6.3	geometry
3	[23]	0.2×0.25	2.54	0.24	-	Maximum	Added
			3.51	0.28	-	gain	inverted L
			4.38	0.2	-	1.98 dB	and T
			5.3	0.57	-	at 2.54 GHz	stub

Table 2. *Cont.*

No.	Paper	Patch Size in λ^2	Resonant freq. (GHz)	BW in GHz ($S_{11} \leq -10$ dB)	Directivity (dB)	Gain (dB)	Techniques
4	[26]	1.12×1.02	28	Total	-	6.9	DRA with
			34	around	-	7.4	slotted
			38	10	-	8.5	ground and
			42	GHz	-	7.5	superstrate
5	[27]	0.93×1.68	28	0.6	-	7.3	4×4
			45	2	-	7.03	hexagonal
			51	1.8	-	7.2	patch
			57	1.3	-	8.0	MIMO
6	This work	0.73×0.9	28.3	0.9	7.8	7.7	Genetic
			38.1	2.3	8.8	8.6	algorithm
			46.6	1.6	7.3	7.2	
			60.0	6.7	7.1	6.9	

6. Conclusions

In this article, the optimization of a quadband microstrip antenna for mm-wave wireless communication employing a genetic algorithm was presented. The proposed antenna resonated at four distinct bands: 27.9 GHz–28.8 GHz, 37.1 GHz–39.4 GHz, 45.9 GHz–47.5 GHz, and 57.8 GHz–64.5 GHz. In all the operating bands, a genetically optimized microstrip antenna performed admirably, attaining a maximum bandwidth of 6.7 GHz at 60.0 GHz with a 7.1 dB directivity and a maximum directivity of 8.8 dB at 38.1 GHz with a 2.3 GHz of bandwidth. A comparison was conducted using related research works presented in the literature to benchmark this antenna. In addition to having sufficient bandwidth, gain, and radiation pattern, the proposed antenna was efficient. As a result, it is a strong contender for wireless mm-wave applications. The paper also demonstrated that a binary-coded genetic algorithm was an excellent candidate for improving the multifunctionality of microstrip antennas with less complexity.

Author Contributions: Conceptualization, A.D. and J.A.; methodology, A.D. and J.J.; software, A.D.; validation, J.A. and M.R.; formal analysis, A.D.; investigation, J.A., J.J., and M.R.; writing—original draft preparation, A.D. and J.J.; writing—review and editing, J.J., M.R. and J.A.; supervision, J.A., M.R. and J.J.; All authors have read and agreed to the published version of the manuscript.

Funding: This research received no external funding.

Institutional Review Board Statement: Not applicable.

Informed Consent Statement: Not applicable.

Data Availability Statement: Data are available in a publicly accessible repository.

Conflicts of Interest: The authors declare no conflict of interest.

References

1. Yeh, C.; Jo, G.D.; Ko, Yo.; Chung, H.K. Perspectives on 6G wireless communications. *ICT Express* **2022**, *in press*. [CrossRef]
2. Xing, Y.; Rappaport, T.S.; Ghosh, A. Millimeter Wave and Sub-THz Indoor Radio Propagation Channel Measurements, Models, and Comparisons in an Office Environment. *IEEE Commun. Lett.* **2021**, *25*, 3151–3155. [CrossRef]
3. Majid, M.; Habib, S.; Javed, A.R.; Rizwan, M.; Srivastava, G.; Gadekallu, T.R.; Lin, J.C.-W. Applications of Wireless Sensor Networks and Internet of Things Frameworks in the Industry Revolution 4.0: A Systematic Literature Review. *Sensors* **2022**, *22*, 2087. [CrossRef]
4. Kamal, M.M.; Yang, S.; Ren, X.; Altaf, A.; Kiani, S.H.; Anjum, M.R.; Iqbal, A.; Asif, M.; Saeed, S.I. Infinity shell shaped MIMO antenna array for mm-wave 5G applications. *Electronics* **2022**, *10*, 165. [CrossRef]
5. Dejen, A.; Ridwan, M.; Anguera, J.; Jayasinghe, J. Millimeter Wave Cellular Communication Performances and Challenges: A Survey. *EAI Endorsed Trans. Mob. Commun. Appl.* **2022**, *7*, e5. [CrossRef]

6. Hussain, W.; Khattak, M.i.; Khattak, M.A.K. Multiband Microstrip Patch Antenna for 5G Wireless Communication. *Int. J. Eng. Work.* **2020**, *7*, 15–21. [CrossRef]

7. Jayasinghe, J.M.J.W.; Uduwawala, D.N.; Anguera, J. Design of Dual Band Patch Antennas for Cellular Communications by Genetic Algorithm Optimization. *Int. J. Eng. Technol.* **2012**, *1*, 26–43. [CrossRef]

8. Hu, C.; Chang, D.; Yu, C.; Hsaio, T.; Lin, D. Millimeter-Wave Microstrip Antenna Array Design and an Adaptive Algorithm for Future 5G Wireless Communication Systems. *Int. J. Antennas Propag.* **2016**, *10*, 7202143. [CrossRef]

9. Anguera, J.; Fernández, A.; Puente, C.; Andújar, A.; Groot, J. Antenna Boosters versus Flexible Printed Circuit Antennas for IoT Devices. *Signals* **2022**, *3*, 326–340. [CrossRef]

10. Simone, M.; Fanti, A.; Mazzarella, G. A Wideband Patch Antenna for 5G. In Proceedings of the IEEE International Symposium on Antennas and Propagation and North American Radio Science Meeting, Montreal, QC, Canada, 5–10 July 2020; pp. 61–62. [CrossRef]

11. Lin, W.; Ziolkowski, R.W.; Baum, T.C. 28 GHz compact omnidirectional circularly polarized antenna for device-to-device communications in the future 5G systems. *IEEE Trans. Antennas Propag.* **2017**, *65*, 6904–6914. [CrossRef]

12. Jeong, M.J.; Abbas, A.; Kim, T.J.; Kim, N. A metasurface-based low-profile wide-band circularly polarized patch antenna for 5G millimeter-wave systems. *IEEE Access* **2020**, *8*, 22127–22135.

13. Zahra, H.; Hussain, M.; Naqvi, S.I.; Abbas, S.M.; Mukhopadhyay, S. A simple monopole antenna with a switchable beam for 5G millimeter-wave communication systems. *Electronics* **2021**, *10*, 2870. [CrossRef]

14. Ullah, H.; Tahir, F.A. A high gain and wide-band narrow-beam antenna for 5G millimeter-wave applications. *IEEE Access* **2020**, *8*, 29430–29434. [CrossRef]

15. Bilal, M.; Naqvi, S.I.; Hussain, N.; Amin, Y.; Kim, N. High-isolation MIMO antenna for 5G millimeter-wave communication systems. *Electronics* **2022**, *11*, 962. [CrossRef]

16. Khalid, M.; Iffat, Naqvi, S.; Hussain, N.; Rahman, M.; Mirjavadi, S.S.; Khan, M.J.; Amin, Y. 4-Port MIMO antenna with defected ground structure for 5G millimeter wave applications. *Electronics* **2020**, *9*, 71. [CrossRef]

17. Tariq, S.; Naqvi, S.I.; Hussain, N.; Amin, Y. A metasurface-based MIMO antenna for 5G millimeter-wave applications. *IEEE Access* **2021**, *9*, 51805–51817. [CrossRef]

18. Hussain, N.; Jeong, M.J.; Abbas, A.; Kim, N. Metasurface-based single-layer wide-band circularly polarized MIMO antenna for 5G millimeter-wave systems. *IEEE Access* **2020**, *8*, 130293–130304. [CrossRef]

19. Dejen, A.; Jayasinghe, J.; Ridwan, M.; Anguera, J. Optimization of Dual-band Microstrip mm-Wave Antenna with Improved Directivity for Mobile Application Using Genetic Algorithm. In Proceedings of the 9th EAI International Conference on Advancements of Science and Technology, Bahirdar, Ethiopia, 27–29 August 2021.

20. Buttazzoni, G.; Comisso, M.; Cuttin, A.; Fragiacomo, M.; Vescovo, R.; Gatti, R.V. Reconfigurable phased antenna array for extending cubesat operations to Ka-band: Design and feasibility. *Acta Astronaut.* **2017**, *137*, 114–121. [CrossRef]

21. Shareef, O.A.; Sabaawi, A.M.A.; Muttair, K.S.; Mosleh, M.F.; Almashhdany, M.B. Design of multi-band millimeter wave antenna for 5G smartphones. *Indones. J. Electr. Eng. Comput. Sci.* **2022**, *25*, 382–387. [CrossRef]

22. Ahmad, A.E.; Floch, J.; Lerideau, G. Quad-Band Antenna for Mobile Communication. In Proceedings of the 6th European Conference on Antennas and Propagation (EUCAP), Prague, Czech Republic, 26–30 March 2012. [CrossRef]

23. Galav, K.; Meena, M.L. DESIGN AND ANALYSIS OF QUAD BAND ANTENNA FOR WIELESS SYSTEMS. *Microelectron. J.* **2020**, *5*, 866–871. [CrossRef]

24. Srivastava, K.; Kumar, A.; Kanaujia, B.K.; Dwari, S.; Kumar, S. Low profile single feed monopole antenna for quad-band circularly polarised applications. *Int. J. Electron.* **2019**, *106*, 318–331. [CrossRef]

25. Abdalla, M.A.; Wahba, W.W.; Atrash, M.E. A quad-band miniaturised compact ϕ-shaped CSRR-based metamaterial-inspired DG resonator antenna. *Int. J. Electron.* **2021**, *109*, 1880–1895. [CrossRef]

26. Sana, M.; Ahmad, S.; Abrar, F.; Qasim, M.A. Millimeter-Wave Quad-Band Dielectric Resonator Antenna for 5G Applications. In Proceedings of the IEEE EUROCON 2021—19th International Conference on Smart Technologies, Lviv, Ukraine, 6–8 July 2021; pp. 304–307. [CrossRef]

27. El-Hassan, M.A.; Farahat, A.E.; Hussein, K.F.A. Millimetric-Wave Quad-Band MIMO Antennas for Future Generations of Mobile Communications. *Prog. Electromagn. Res. B* **2022**, *95*, 41–60. [CrossRef]

28. Abdelatif, N.; Zamel, H.; Attiya, A.; Awamry, A. Multi-Band mm-Wave Antenna for 5G-WiGig Communication Systems. *Prog. Electromagn. Res. C* **2020**, *99*, 133–143. [CrossRef]

29. Almashhdany, M.B.; Al-Ani, O.A.; Sabaawi, A.M.A. Design of Multi-band Slotted mm-Wave Antenna for 5G Mobile Applications. In Proceedings of the 3rd International Conference on Sustainable Engineering Techniques (ICSET 2020), Baghdad, Iraq, 17 June 2020.

30. Ding, W.; Meng, F.; Tian, Y.; Yuan, H. Antenna Optimization Based on Auto-Context Broad Learning System. *Int. J. Antennas Propag.* **2022**, *2022*, 7338164. [CrossRef]

31. Zhang, X.; Tian, Y.; Zheng, X. Antenna Optimization Design Based on Deep Gaussian Process Model. *Int. J. Antennas Propag.* **2020**, *2020*, 2154928. [CrossRef]

32. Kapoor, A.; Mishra, R. Genetic Algorithm Optimized Gain Augmented Dual Band Printed Antenna for Cognitive eHealth Care (IoMT) Applications. In Proceedings of the 2022 IEEE 11th International Conference on Communication Systems and Network Technologies (CSNT), Indore, India, 23–24 April 2022; pp. 6–11. [CrossRef]

33. Dejen, A.; Ridwan, M.; Jayasinghe, J.; Anguera, J. Multi-Band mm-Wave Wearable Antenna Synthesized with a Genetic Algorithm. *Int. J. Antennas Propag.* **2022**, *2022*, 1958247. [CrossRef]

34. Balanis, C.A. *Modern Antenna Handbook*; John Wiley and Sons Inc.: Hoboken, NJ, USA, 2013.

35. Haupt, R.L. An Introduction to Genetic Algorithms for Electromagnetics. *IEEE Antennas Propag. Mag.* **1995**, *37*, 7–15. [CrossRef]

36. Saraereh, O.A.; Saraira, A.A.A.; Alsafasfeh, Q.H.; Arfoa, A. Bio-Inspired Algorithms Applied on Microstrip Patch Antennas: A Review. *Int. J. Commun. Antenna Propag.* **2016**, *6*, 336–347. [CrossRef]

37. Johnson, J.M.; Rahmat-Samii, Y. Genetic Algorithms in Engineering Electromagnetics. *IEEE Antennas Propag. Mag.* **1997**, *39*, 7–21. [CrossRef]

38. Dejen, A.; Jayasinghe, J.; Ridwan, M.; Anguera, J. Genetically engineered tri-band microstrip antenna with improved directivity for mm-wave wireless application. *AIMS Electron. Electr. Eng.* **2022**, *6*, 1–15. [CrossRef]

39. Jayasinghe, J.M.J.W.; Anguera, J.; Uduwawala, D.N. A simple design of multi band microstrip patch antennas robust to fabrication tolerances for GSM, UMTS, LTE, and Bluetooth applications by using genetic algorithm optimization. *Prog. Electromagn. Res. M* **2012**, *27*, 255–269. [CrossRef]